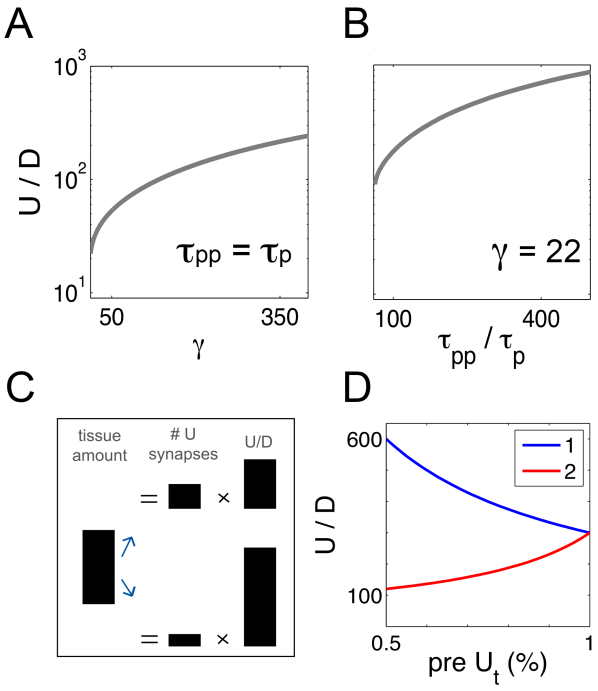

Figure S1. Protein synthesis and synaptic dwell-time both affect the proportional level of total kinase in L-LTP and naïve state. **(A)** Increasing γ, the synthesis up-regulation factor, increases U/D where U and D are amounts of total kinase in single synapse in the upper (L-LTP) and lower (naïve) stable solutions such as in Fig. 1B. **(B)** Increasing synaptic dwell-times proportionally (τ_{pp}/τ_p) also increases U/D. **(C)** The amount of increase in total homogenate is related to the change in a single synapse. When fewer synapses have U amount, a larger increase in single synapse (U/D) is needed to account for the same amount of increase in the tissue. **(D)** Percentage of synapses in the tissue with U amount (U_t) could be used to estimate U/D. Blue (1) curve results if we assume U_t doubles after stimulation. Red (2) curve results if we assume U_t = 2% after stimulation, regardless of the level of U_t prior to stimulation (pre U_t).

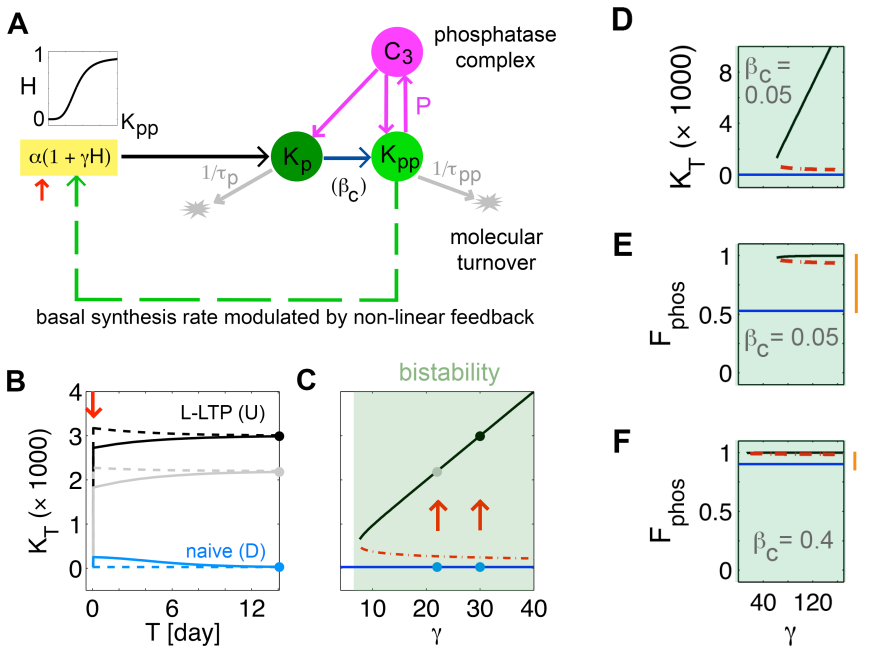

Figure S2. Model with constant phosphorylation and feedback at the level of protein synthesis. Constant phosphorylation can be obtained either via an external kinase or (cis)autophosphorylation. **(A)** Schematic diagram of the model. K_p and K_{pp} are singly and doubly phosphorylated kinase with turnover times, τ_p and τ_{pp}. C_3 is a complex resulting from binding of K_{pp} with free phosphatase P. α and $\gamma\alpha$ are synthesis rates of K_p during pre and post potentiation, and β_c is the rate of phosphorylation. H is a Hill function of order 4 used for non-linear modulation of protein synthesis. Red arrows in all panels indicate induction protocol: 15 min of elevated synthesis rates in the range 2-3.5 units/s. **(B)** Time evolution of total amount of the kinase, K_T, with or without induction for γ = 22 (gray) and 30 (black). U and D indicate potentiated synaptic state (L-LTP) and pre-potentiated (naïve) synaptic state. Solid lines are from weaker stimulation during induction than dashed lines. Circles indicate equilibria (steady states) achieved over time. **(C)** Bifurcation diagram showing dependence of equilibria on γ. Blue and black curves are composed of equilibria of type D and U. Circles indicate particular cases in panel B. Red dashed curve represent threshold or unstable equilibria. Green-shaded box indicate region of bi-stability ("molecular switch"). **(D)** Equilibria in terms of total kinase, K_T, with respect to control parameter, γ, for activity-dependent protein synthesis while phosphorylation rate is set low at β_c = 0.05. In all panels, shaded regions indicate bi-stability, blue lines are D states, black lines are U states, and red dashed lines are thresholds for switching between the two states. **(E)** For the same parameters as in panel A, equilibria in terms of fraction of phosphorylation, F_{phos}, are plotted. When present, vertical orange bars in all panels indicate change due to stimulation. **(F)** Same as panel E except β_c = 0.4.

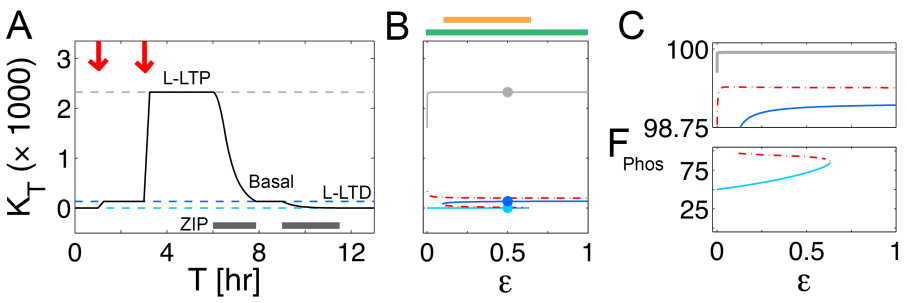

Figure S3. Bistability can exist for a wide range of feedback autophosphorylation rate, ε, in the hybrid model but multistability may emerge due to multiple feedback mechanisms. **(A)** Starting from lowest possible total kinase, K_T, stimulations with varying strength (red arrows) reveal three persistent states: L-LTD (cyan dashed), naïve (blue dashed), L-LTP (grey dashed). Simulated ZIP could both reverse L-LTP and induce L-LTD. **(B)** Bifurcation diagram with respect to autophosphorylation rate, ε, shows bistability and multistability are robust to approximately 90% and 50% variation (green and yellow bars on top) respectively if other phosphorylation parameters are small (β_t = 0.1 s^{-1} and β_c = 0). Solid lines are stable equilibriums resistant to changes in time; dashed lines are unstable equilibriums or thresholds. **(C)** Feedback autophosphorylation could account for the desired fraction of phosphorylation, F_{Phos}. Small change (~1%) in F_{Phos} is seen from naïve (blue curve) to L-LTP (gray curve) state; however, a greater than 20% change is seen from L-LTD (cyan curve) to naïve state.

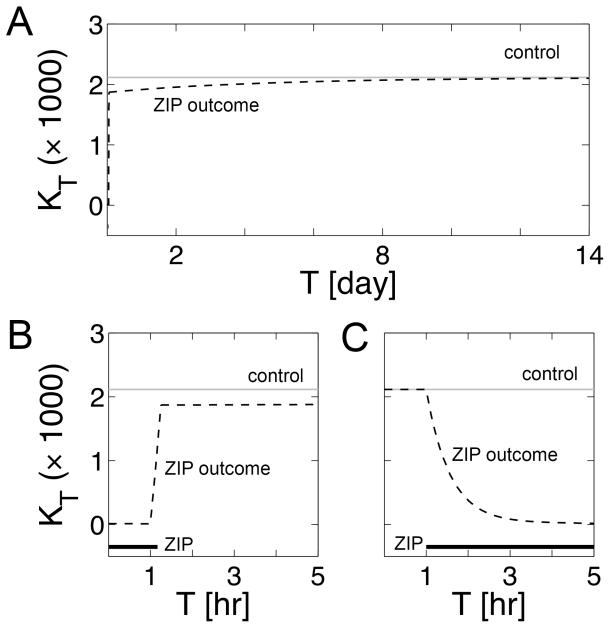

Figure S4. Effects of ZIP stay consistent in the absence of autophosphorylation. **(A-B)** Application of ZIP during induction does not prevent L-LTP but slows down convergence to the steady state (close up shown in B). **(C)** Post stimulation application of ZIP reverses L-LTP. Dashed line is dynamics with ZIP; gray line is control that was previously potentiated. The presence of ZIP during stimulation was simulated by setting $\gamma = 0$ and $\tau_{pp} = 2000$ (s). In panel B ZIP lasted until half the time of 15-min elevated synthesis and in panel C it was applied for 4-hr (indicated by Horizontal bars).

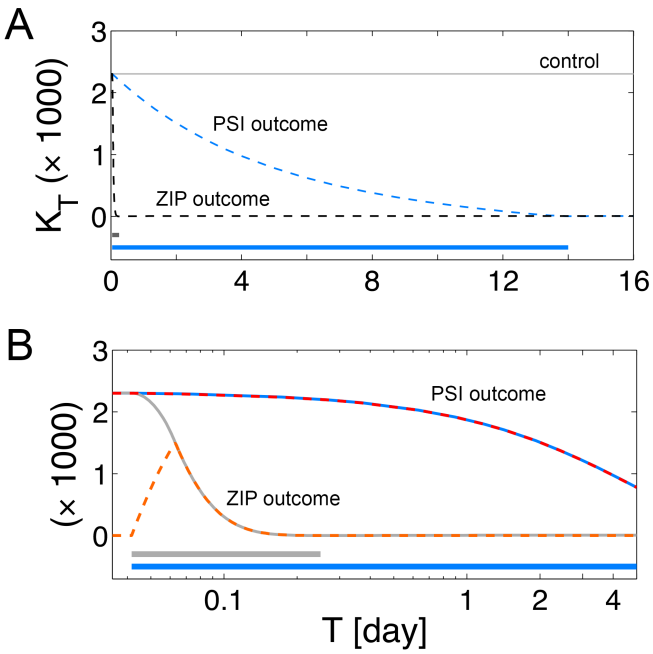

Figure S5. Long-term application of PSI reverses L-LTP, and this reversal can be explained by synaptic dwell-time of doubly phosphorylated kinase. **(A)** A 2-week long simulation of PSI ($\alpha = \gamma = 0$ for duration of blue horizontal bar) reverses L-LTP as well as 3-hour long simulation of ZIP ($\varepsilon = \beta = \gamma = 0$ for duration of gray horizontal bar). Control shows L-LTP without inhibitors. **(B)** The time evolution of K_T in the presence of ZIP and PSI superimposed with those of K_p (orange dashed) and K_{pp} (red dashed) during the same simulations. Blue and gray traces are concentrations of K_T. Horizontal bars indicate duration of inhibitors: PSI (blue) and ZIP (gray). Note that we used a log scale so both simulations can be observed on the same plot.

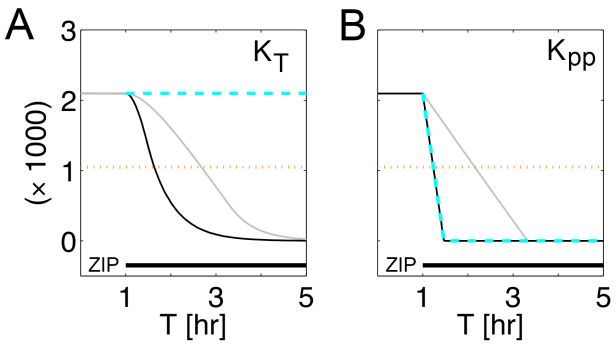

Figure S6. Reducing phosphatase activity slows the time course of L-LTP reversal by ZIP and clamping all other reactions in the hybrid model shows that reversal is led by phosphatase activity. **(A)** Level of total kinase K_T during reversal of L-LTP. ZIP is applied starting at 1 hour with full (black line) or reduced (gray line) phosphatase activity. To simulate the reduction of phosphatase activity we assumed that its concentration was reduced by a factor of 5 compared to the black trace. Parameters for black trace are the same as Fig. 2D. Application of ZIP is implemented by loss of phosphorylation and feedback protein synthesis for the period of time indicated by horizontal bars. Orange dotted lines indicate half the concentrations of the initial state. Cyan dashed lines result from intact phosphatase activity while phosphorylation, synthesis and degradation are blocked for the case in Fig. 2D. **(B)** Level of doubly phosphorylated kinase, K_{pp}, corresponding to panel A. For the parameters in Fig. 2D (solid black trace), decay of K_{pp} matches that resulting from the sole activity of phosphatase (cyan dashed trace).

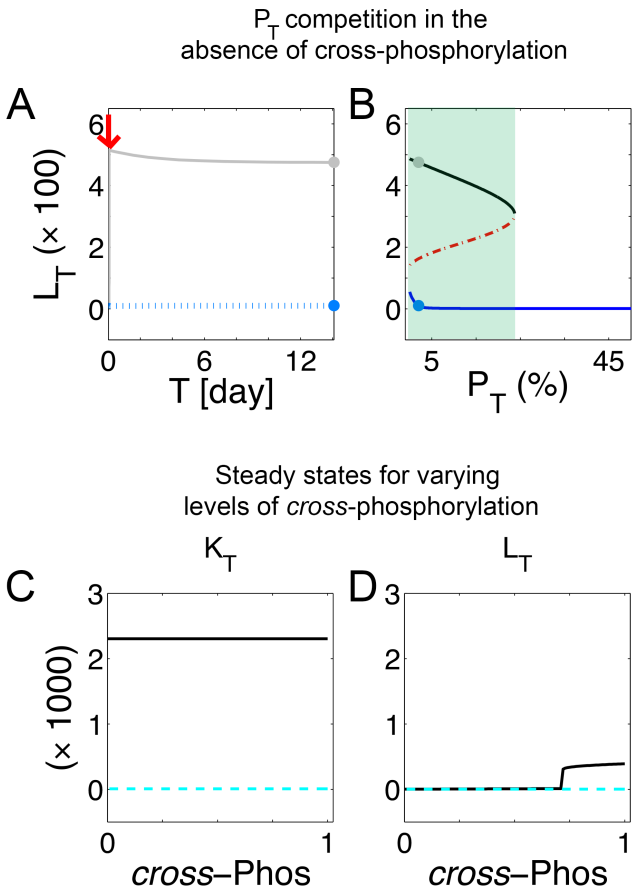

Figure S7. Competition for phosphatase and cross-phosphorylation independently can induce bi-stability in otherwise mono-stable kinase. **(A)** Gray (but not blue) trace received stimulation (red arrow) showing persist up-regulation of kinase L similar to that in the presence of kinase K (shown in Fig. 5B). Circles indicate naïve (blue) and L-LTP (gray) synaptic states. **(B)** Bifurcation diagram for kinase L with respect to total phosphatase P_T. Stable L-LTP states (black) and naive states (blue) separated by unstable threshold state (red dashed). Circles indicate the specific case in panel A, showing reduction in phosphatase (due to competition) can lead to bi-stability (shaded region) or 'molecular switch' mechanism. **(C-D)** Numerically computed stable steady states in the two-kinase model are plotted with respect to a parameter introduced for controlling the level of cross-phosphorylation (efficiency of phosphorylation of K species by L species and vice versa), while a parameter introduced for the competition for phosphatase was set to zero. Black curve is composed of L-LTP states; cyan dashed curve is composed of naïve states. Kinase L achieves significantly higher L-LTP state at high degree of cross-phosphorylation (cross-Phos). Note that we assumed kinase L is less efficient (slower reaction) at phosphorylation than kinase K.

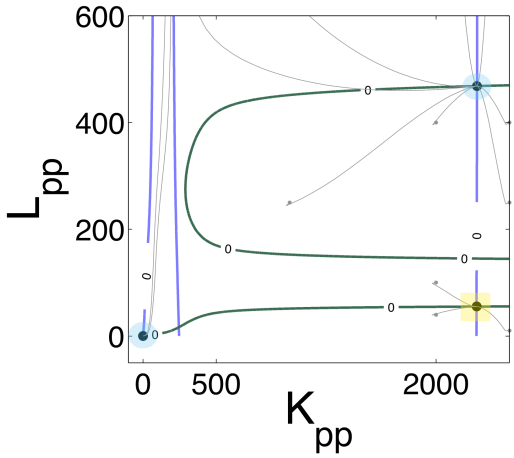

Figure S8. Mathematical analysis verifies steady states identified by long-term numerical dynamics or solutions. Green and blue curves are nullclines, nL = 0 and nK = 0, respectively (see the section 'finding of steady state analytically' below). The intersections are analytical steady states. Black circles are numerical steady states found by long-term dynamics and verified to be stable via evaluation of the Jacobian of the Ordinary Differential Equations (ODEs) describing the full model. Gray trajectories are dynamics resulting from various initial (gray dots) concentrations of K_{pp} and L_{pp}. Blue shaded steady states are depicted in Fig. 5B and the yellow shaded steady state is only observable if kinase L is blocked (not synthesized) during the induction protocol. In general we assume the pool of free phosphatase is equally likely to bind both kinases (i.e., competitive) and cross-phosphorylation occurs at maximal capacity (reactions involving kinase L are slower than those with only kinase K).

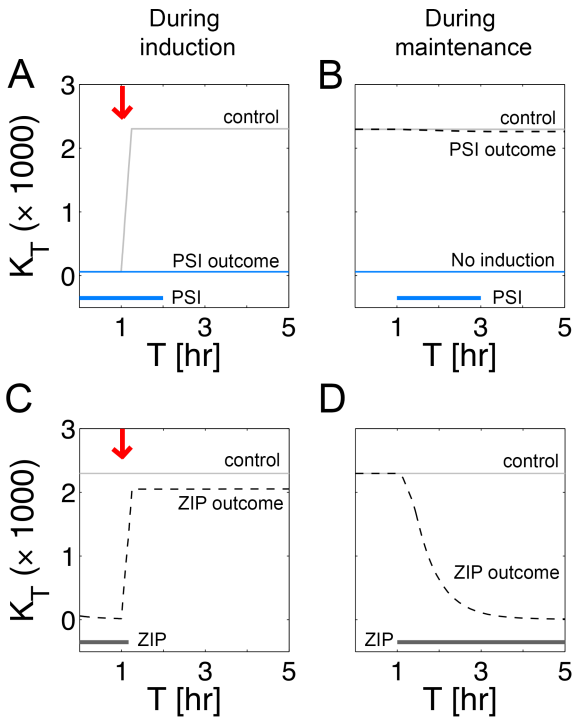

Figure S9. If synaptic dwell-times vary (τ_{pp} >> τ_p), feedback (trans)autophosphorylation is sufficient to account for differential effects of kinase and protein synthesis inhibitors, and for different concentrations of total kinase in the lower and upper stable states. This model, however, cannot attain minimal change in fraction of phosphorylation with robustness to changes in parameters. **(A)** Grey line (control) indicates effect of induction without PSI; blue line (PSI outcome) indicates effect of induction with PSI. Red arrows in all panels when present indicate 15-min of artificially elevated synthesis. Thick horizontal lines at the bottom indicate durations of inhibitor application in all panels. **(B)** Grey line (control) is synaptic state in L-LTP, black dashed line (PSI outcome) indicates effect of PSI on previously potentiated state, and blue line (no induction) indicates naïve synaptic state. **(C)** Grey line (control) is effect of induction without ZIP (induced prior to red arrow); black dashed line (ZIP outcome) is effect of induction (induce at red arrow) with ZIP, which is applied for 7.5 min from the start of induction. **(D)** Grey line (control) previously potentiated synaptic state; black dashed line (ZIP outcome) is the effect of ZIP application on previously potentiated state. PSI is simulated by setting $\alpha = 0$, and ZIP is simulated by setting $\varepsilon = 0$.

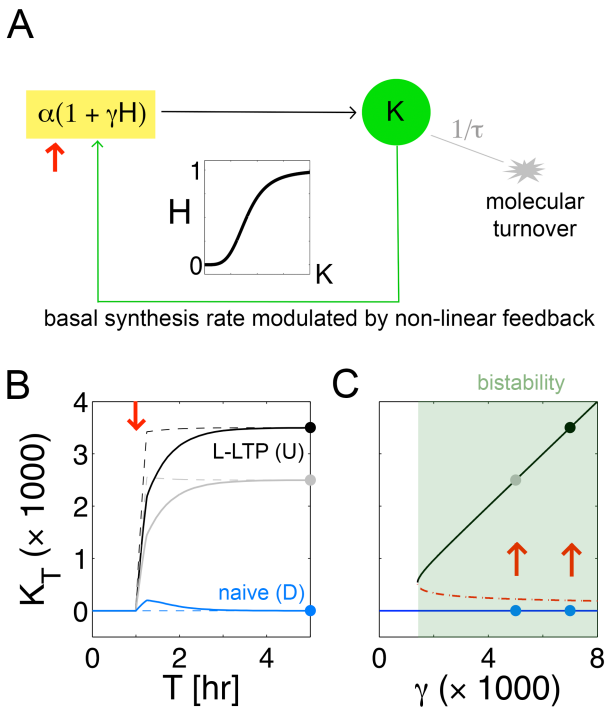

Figure S10. "Molecular switch" can be instantiated by a kinase model that has single form and protein synthesis based self-regulation; however, it cannot account for the differential effects of synthesis and kinase inhibitors (see Fig. S11), or the fractional phosphorylation. **(A)** Schematic representation of the model for a kinase, K, which has lifetime, τ, in the synaptic compartment and is produced in an activity-dependent manner, indicated by the function H. Red arrows in all panels indicate 15 minutes of elevated synthesis (stimulus). **(B)** Sufficiently strong stimulus (dashed lines) persistently increases concentration of the total kinase, K_T, in naïve synapse, D, to that of potentiated synapse, U. Solid lines show varying levels of stimuli. **(C)** Bifurcation diagram: equilibria resulting from given values of magnitude of activity-dependent protein synthesis, γ. Black and blue solid lines indicate U and D states. Red dashed line indicates threshold for switching between the two states. Circles indicate the specific cases in B. The ordinary differential equation for this model is $\dot{K} = \alpha(1 + \gamma H) - K/\tau$, where $H = \frac{K^4}{K_{1/2}^4 + K^4}$ and K = K_T.

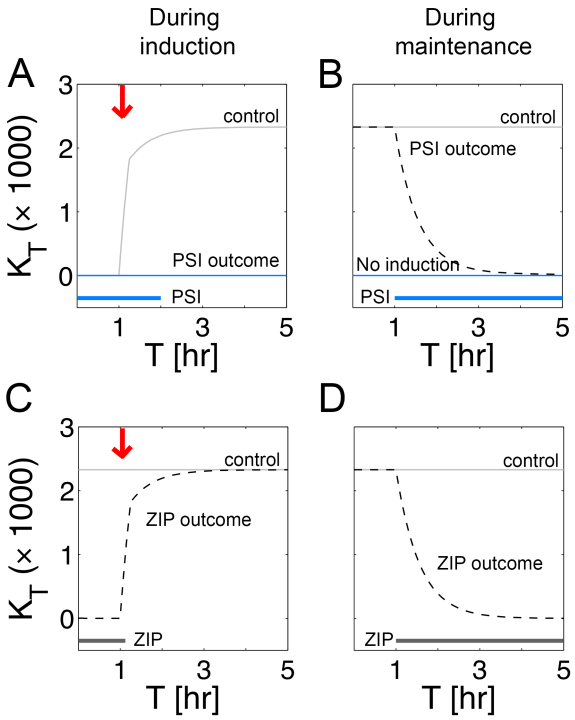

Figure S11. If we consider one-state kinase (see Fig. S11) or the same synaptic dwell-time ($\tau_{pp} = \tau_p$), differential effects of kinase and protein synthesis inhibitors are violated, and such models fail to account for all key experimental observations. **(A)** Grey line (control) indicates effect of induction without PSI; blue line (PSI outcome) indicates effect of induction with PSI. Red arrows in all panels when present indicate 15 min of artificially elevated synthesis. Thick horizontal lines at the bottom indicate durations of inhibitor application in all panels. **(B)** Grey line (control) is synaptic state in L-LTP, black dashed line (PSI outcome) indicates effect of PSI on previously potentiated state, and blue line (no induction) indicates naïve synaptic state. **(C)** Grey line (control) is effect of induction without ZIP (induced prior to red arrow); black dashed line (ZIP outcome) is effect of induction (induce at red arrow) with ZIP, which is applied for 7.5 min from the start of induction. **(D)** Grey line (control) previously potentiated synaptic state; black dashed line (ZIP outcome) is the effect of ZIP application on previously potentiated state. PSI is simulated by setting $\alpha = \gamma = 0$, and ZIP is simulated by setting $\varepsilon = \beta_{t,c} = \gamma = 0$ when present.

Parameters for figures

Unless otherwise mentioned, the following parameters are the same in all figures: $r_1 = 1$ s^{-1}, $r_{-1} = 1/50$ s^{-1}, $r_2 = 1$ s^{-1}, $r_3 = 1/20$ s^{-1}, $r_{-3} = 1/10$ s^{-1}, $r_4 = 1/20$ s^{-1}, $P_T = 25$, $\beta_c = 0$. In Fig. S2 B,C $\beta_c = 2$, and in Fig. S4 $\beta_c = 1.2$. In Fig. S6 $P_T = 5$ for gray curve. None of the above parameters are present in Fig. S11.

	Fig. S1	Fig. S2	Fig. S3	Fig. S4	Fig. S5	Fig. S6
α [s^{-1}]	1/4,000	1/4,000	1/4,000	1/4,000	1/4,000	1/4,000
γ	Varies (A), 22 (B)	22 (B), 30 (B), varies (C-F)	22	22	22	22
$K_{1/2}$	2	400	400	400	400	400
ε [s^{-1}]	0	0	1/2 (A), varies (B,C)	0	1/200	0
β_t [s^{-1}]	1/10	0	1/10	0	1	1
τ_p [s]	2,000	2,000	2,000	2,000	2,000	2,000
τ_{pp} [s]	2,000 (A), varies (B)	400,000	400,000	400,000	400,000	400,000

	Fig. S7	Fig. S8,9 (K)	Fig. S8,9 (L)	Fig. S10	Fig. S11	Fig. S12
α [s^{-1}]	1/4,000	1/4,000	1/4,000	1/200	1/4,000	1/4,000
γ	22	22	8	0	5000 (B), 7000 (B), varies (C)	4600
$K_{1/2}$	400	400	200	2	400	400
ε [s^{-1}]	1/200	1/200	1/2000	1/6250	*none*	1
β_t [s^{-1}]	1	1	1/10	1/89	*none*	1
τ [s]	*none*	*none*	*none*	*none*	2,000	*none*
τ_p [s]	2,000	2,000	2,000	2,000	*none*	2,000
τ_{pp} [s]	400,000	400,000	222,222	666,667	*none*	2,000

Percent change: Tissue to synapse

Derivation of percent change for a single synapse (U/D) from that of a tissue (ρ) where n_u is the number of pre-existing potentiated synapses containing U amount, $(n_{total} - n_U)$ is the number of naïve synapses containing D amount, n_{LTP} is the number of synapses potentiated due to experimental stimulation, n_{total} is the total number of synapses in the tissue, and R is the total extra-synaptic protein, which is assumed to remain unaltered.

$$\begin{aligned}
\rho &= \frac{(n_U + n_{LTP})U + (n_{total} - n_U - n_{LTP})D + R}{n_U U + (n_{total} - n_U)D + R} \\
&= 1 + \frac{n_{LTP}U - n_{LTP}D}{n_U U + (n_{total} - n_U)D + R} \\
(\rho - 1) &= \frac{n_{LTP}(U - D)}{n_U U + (n_{total} - n_U)D + R} \\
U(n_{LTP} - n_U(\rho - 1)) &= D((n_{total} - n_U)(\rho - 1) + n_{LTP}) + R(\rho - 1) \\
\frac{U}{D} &= \frac{(n_{total} - n_U)(\rho - 1) + n_{LTP}}{(n_{LTP} - n_U(\rho - 1))} + \frac{R(\rho - 1)}{D(n_{LTP} - n_U(\rho - 1))} \\
&= 1 + \frac{n_{total}(\rho - 1)}{(n_{LTP} - n_U(\rho - 1))} + \frac{R(\rho - 1)}{D(n_{LTP} - n_U(\rho - 1))} \\
&= 1 + \frac{1 + R/(Dn_{total})}{\frac{1}{(\rho - 1)}\, n_{LTP}/n_{total} - n_U/n_{total}}
\end{aligned}$$

Model calibration for the amount of protein was based on experimental observation 1 in the Introduction. Experiments found atypical PKCs increase by nearly 75% after L-LTP induction; however, the percent increases reported in experiments are from hippocampal CA1 area tissue homogenate, which contain many synapses. In addition, extra-synaptic compartments of neurons also contain atypical PKCs (Hernandez et al. 2014). The total concentration of an atypical PKC before L-LTP is: $n_u U + (n_{total} - n_U)D + R$, and after L-LTP is $(n_u + n_{LTP})U + (n_{total} - n_U - n_{LTP})D + R$, where n_u is the number of pre-existing potentiated synapses containing U amount, $(n_{total} - n_U)$ is the number of naïve

synapses containing D amount, n_{LTP} is the number of synapses potentiated due to experimental stimulation, n_{total} is the total number of synapses in the tissue, and R is the total extra-synaptic protein, which is assumed to remain unaltered during the experiment. Therefore, the ratio of the atypical PKC amount in the L-LTP state (U) to that of the naïve state (D) in the single synapse is: $\frac{U}{D} = 1 + (1 + \frac{R/D}{n_{total}})/(\frac{1}{(\rho-1)}\frac{n_{LTP}}{n_{total}} - \frac{n_U}{n_{total}})$ where ρ is the percent increase in the tissue and the derivation is shown in the Appendix. In order to determine U/D from the experimental data we must know the percentage of synapse that were in L-LTP state both before and after stimulation, and the proportion of extra-synaptic atypical PKC to the total synaptic amount in the tissue if all of the synapses were in naïve state. In Fig. S1 we show graphically how U/D depends on $\frac{n_U}{n_{total}}$ (referred as pre U_t in the figure) for two different series of values of $\frac{n_{LTP}}{n_{total}}$ assuming R=0. For R≠0 the graphs in S1 will only be scaled vertically.

Finding of steady states analytically

The whole reaction network is represented by a system of 14 ODEs. In order to find the steady states analytically, each ODE is set to zero and solved for the 14 variables in the system.

$$\begin{aligned}
\frac{dK_p}{dt} &= H_{Kpp} - (\lambda_1 + r_5)K_p + r_4 C_3^K - (2r_1\beta K_p K_p + r_1\epsilon K_p K_{pp}) \\
&\quad + 2r_{-1}C_1^K + r_2 C_1^K + r_{-1}C_2^K \\
&\quad + \delta_7(-((2r_1\beta(1+\delta_1)K_p L_p) + \epsilon(1+\delta_2)r_1 K_p L_{pp}) \\
&\quad + r_{-1}C_{\times 1}^K + r_2 C_{\times 1}^L + r_{-1}C_{\times 2}^K + r_{-1}C_{\times 1}^L) \qquad (1) \\
\frac{dK_{pp}}{dt} &= r_5 K_p - \lambda_2 K_{pp} - r_3(P_t - C_3^K - C_3^L)K_{pp} + r_{-3}C_3^K \\
&\quad - \epsilon r_1 K_{pp} K_p + r_2 C_1^K + (r_{-1} + 2r_2)C_2^K \\
&\quad + \delta_7(-\epsilon(1+\delta_2)r_1 L_p K_{pp} + r_2 C_{\times 2}^K + r_{-1}C_{\times 2}^L + r_2 C_{\times 2}^L + r_2 C_{\times 1}^K) \qquad (2) \\
\frac{dC_1^K}{dt} &= r_1\beta K_p K_p - (r_{-1} + r_2)C_1^K \qquad (3) \\
\frac{dC_{\times 1}^K}{dt} &= \delta_7(r_1\beta(1+\delta_1)K_p L_p - (r_{-1} + r_2)C_{\times 1}^K) \qquad (4) \\
\frac{dC_2^K}{dt} &= r_1\epsilon K_{pp} K_p - (r_{-1} + r_2)C_2^K \qquad (5) \\
\frac{dC_{\times 2}^K}{dt} &= \delta_7(\epsilon(1+\delta_2)r_1 K_p L_{pp} - (r_{-1} + r_2)C_{\times 2}^K) \qquad (6) \\
\frac{dC_3^K}{dt} &= r_3(P_t - C_3^K - C_3^L)K_{pp} - (r_{-3} + r_4)C_3^K \qquad (7) \\
\frac{dL_p}{dt} &= H_{Lpp} - (\lambda_1(1+\delta_8) + r_5)L_p + r_4 C_3^L - (2r_1\beta(1+\delta_1)L_p L_p + \epsilon(1+\delta_2)r_1 L_p L_{pp}) \\
&\quad + 2r_{-1}C_1^L + r_2 C_1^L + r_{-1}C_2^L \\
&\quad + \delta_7(-((2r_1\beta(1+\delta_1)L_p K_p) + \epsilon(1+\delta_2)r_1 L_p K_{pp}) \\
&\quad + r_{-1}C_{\times 1}^L + r_2 C_{\times 1}^K + r_{-1}C_{\times 2}^L + r_{-1}C_{\times 1}^K) \qquad (8) \\
\frac{dL_{pp}}{dt} &= r_5 L_p - (\lambda_2(1+\delta_6))L_{pp} - r_3(P_t - C_3^K - C_3^L)L_{pp} + r_{-3}C_3^L \\
&\quad - \epsilon(1+\delta_2)r_1 L_{pp} L_p + r_2 C_1^L + (r_{-1} + 2r_2)C_2^L \\
&\quad + \delta_7(-\epsilon(1+\delta_2)r_1 K_p L_{pp} + r_2 C_{\times 2}^L + r_{-1}C_{\times 2}^K + r_2 C_{\times 2}^K + r_2 C_{\times 1}^L) \qquad (9) \\
\frac{dC_1^L}{dt} &= r_1\beta(1+\delta_1)L_p L_p - (r_{-1} + r_2)C_1^L \qquad (10) \\
\frac{dC_{\times 1}^L}{dt} &= \delta_7(r_1\beta(1+\delta_1)L_p K_p - (r_{-1} + r_2)C_{\times 1}^L) \qquad (11) \\
\frac{dC_2^L}{dt} &= \epsilon(1+\delta_2)r_1 L_{pp} L_p - (r_{-1} + r_2)C_2^L \qquad (12) \\
\frac{dC_{\times 2}^L}{dt} &= \delta_7(\epsilon(1+\delta_2)r_1 L_p K_{pp} - (r_{-1} + r_2)C_{\times 2}^L) \qquad (13) \\
\frac{dC_3^L}{dt} &= r_3(P_t - C_3^K - C_3^L)L_{pp} - (r_{-3} + r_4)C_3^L \qquad (14)
\end{aligned}$$

Rearranging easily solves equations 3-6 and 10-13, and the linear algebraic method of elimination solves equation 7 and 14.

$$C_1^K = (K_p^2 \beta r_1)/(r_2 + r_{-1}) \quad (1)$$
$$C_{\times 1}^K = (K_p L_p \beta r_1 (\delta_1 + 1))/(r_2 + r_{-1}) \quad (2)$$
$$C_2^K = (K_p K_{pp} \epsilon r_1)/(r_2 + r_{-1}) \quad (3)$$
$$C_{\times 2}^K = K_p L_{pp} \epsilon r_1 (\delta_2 + 1))/(r_2 + r_{-1}) \quad (4)$$
$$C_3^K = (K_{pp} P_t r_3)/(r_4 + r_{-3} + K_{pp} r_3 + L_{pp} r_3) \quad (5)$$
$$C_1^L = (L_p^2 \beta r_1 (\delta_1 + 1))/(r_2 + r_{-1}) \quad (6)$$
$$C_{\times 1}^L = (K_p L_p \beta r_1 (\delta_1 + 1))/(r_2 + r_{-1}) \quad (7)$$
$$C_2^L = (L_p L_{pp} \epsilon r_1 (\delta_2 + 1))/(r_2 + r_{-1}) \quad (8)$$
$$C_{\times 2}^L = (K_{pp} L_p \epsilon r_1 (\delta_2 + 1))/(r_2 + r_{-1}) \quad (9)$$
$$C_3^L = (L_{pp} P_t r_3)/(r_4 + r_{-3} + K_{pp} r_3 + L_{pp} r_3) \quad (10)$$

In order to solve for the remaining variables, we consider the following sum of ODEs, which results in simple expressions.

$$\frac{dK_p}{dt} + \frac{dK_{pp}}{dt} = H_{Kpp} - K_p \lambda_1 - K_{pp} \lambda_2 \quad (1)$$
$$\frac{dL_p}{dt} + \frac{dL_{pp}}{dt} = H_{Lpp} - L_p \lambda_1 - L_{pp} \lambda_2 - L_p \delta_8 \lambda_1 - L_{pp} \delta_6 \lambda_2 \quad (2)$$

The above expressions can be used to solve for K_p and L_p, giving us the following constraints.

$$Kp = H_{Kpp}/\lambda_1 - K_{pp} \lambda_2/\lambda_1 \geq 0 \quad (1)$$
$$Lp = H_{Lpp}/(\lambda_1 + \delta_8 \lambda_1) - L_{pp}(\lambda_2 + \delta_6 \lambda_2)/(\lambda_1 + \delta_8 \lambda_1) \geq 0 \quad (2)$$

Using parameters from Fig. 5A, we get the following bounds on K_{pp} and L_{pp}.

$$Kp = 11.5 - K_{pp}0.005 \geq 0 \quad (1)$$
$$Lp = 4.5 - L_{pp}0.009 \geq 0 \quad (2)$$

which translates to $K_{pp} \leq 2300$ and $L_{pp} \leq 500$. Finally, we consider the following differences of ODEs.

$$nK = \frac{dK_p}{dt} - \frac{dK_{pp}}{dt} \quad (1)$$
$$nL = \frac{dL_p}{dt} - \frac{dL_{pp}}{dt} \quad (2)$$

If nK = 0 and nL = 0, then the ODEs 1, 2 and 8, 9 are guaranteed to be zeros making the full system of ODEs to be zeros at the same time. Hence, the intersections of the implicit curves resulting from nK = 0 and nL = 0 are the steady states. Fig. S11 shows these curves, along with numerically integrated solutions.

Bibliography

Hernandez AI, Oxberry WC, Crary JF, Mirra SS, Sacktor TC. 2014. Cellular and subcellular localization of PKM zeta. *Philos Trans R Soc B Biol Sci* **369**: 20130140.